

Balance Control of a Novel Wheel-legged Robot: Design and Experiments

Shuai Wang^{1,*}, Leilei Cui^{2,*}, Jingfan Zhang³, Jie Lai¹, Dongsheng Zhang¹, Ke Chen¹,
Yu Zheng¹, Zhengyou Zhang¹, *Fellow, IEEE*, and Zhong-Ping Jiang², *Fellow, IEEE*

Abstract— This paper presents a balance control technique for a novel wheel-legged robot. We first derive a dynamic model of the robot and then apply a linear feedback controller based on output regulation and linear quadratic regulator (LQR) methods to maintain the standing of the robot on the ground without moving backward and forward mightily. To take into account nonlinearities of the model and obtain a large domain of stability, a nonlinear controller based on the interconnection and damping assignment - passivity-based control (IDA-PBC) method is exploited to control the robot in more general scenarios. Physical experiments are performed with various control tasks. Experimental results demonstrate that the proposed linear output regulator can maintain the standing of the robot, while the proposed nonlinear controller can balance the robot under an initial starting angle far away from the equilibrium point, or under a changing robot height.

I. INTRODUCTION

Wheel-legged robots [1] [2] combine the advantages of wheeled robots and legged robots, that possess the high energy-efficiency of wheels and the strong adaptability to overcome uneven terrain and obstacles using legs. Bipedal wheeled robots arouse our interests because of their agility and potential opportunities in the practical applications. However, they are unstable systems with only two contact points between the ground and the wheels/legs. Besides, the possible nonlinearities and uncertainties, such as unknown equilibrium state, nonlinear system model and posture change (height change), make the balance control more challenging. In this work, we control a novel wheel-legged robot in Fig. 1 by both linear and nonlinear controllers, and the performance is tested by a variety of experiments.

A. Related Work

Bipedal wheeled robots are unstable underactuated systems. The existing balancing control methods include using the traditional linearized model [3], or whole-body dynamics control [4], in the case where the robot keeps a constant

*This work is supported in part by the National Science Foundation under Grant EPCN-1903781. The first two authors contributed equally to this work.

¹S. Wang, J. Lai, D. Zhang, K. Chen, Y. Zheng and Z. Zhang are with Tencent Robotics X, Tencent Holdings, Shenzhen, Guangdong, China (e-mail: shawnwang@tencent.com)

²L. Cui and Z. P. Jiang are with the Control and Networks Lab, Department of Electrical and Computer Engineering, Tandon School of Engineering, New York University, Brooklyn, NY 11201 USA (e-mail: l.cui@nyu.edu; zjiang@nyu.edu)

³J. Zhang is with Department of Electrical & Electronic Engineering, School of Engineering, University of Manchester, M13 9PL, UK. (e-mail: jingfan.zhang@manchester.ac.uk)

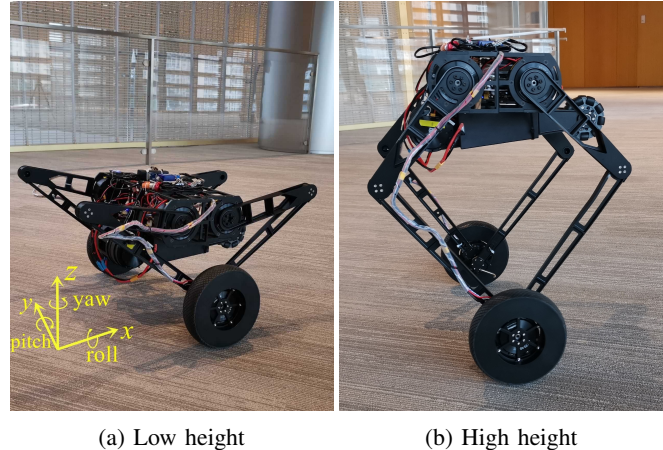


Fig. 1: The novel wheel-legged robot

height. A milestone of the development of bipedal wheeled robot is Handle [1] by Boston Dynamics. Handle can finish a few tasks like truck unloading, order building and palletizing while keeping balanced. Unfortunately, little technical detail has been released. Recently, ETH Ascento and its LQR-assisted control are described in [2] and [5]. Its whole-body control scheme shows robustness to disturbances by active compliance to uneven terrain.

A practical difficulty of these two-wheeled robots is that the equilibrium is often not the upward direction due to the uneven mass distribution of the robot or the installation error of the sensors. Therefore, it is hard to provide a reference position for the balance control. As a consequence, keeping the robot standstill is formidable. In this case, output regulation theory is an appropriate tool to force the system output to a desired state under unknown disturbances; see, e.g., [6], [7] and theoretical applications to robot manipulators [8], [9], but it is less common to see practical applications in mobile robotic systems. Besides, nonlinear output regulation is challenging because regulator equations are nonlinear partial differential equations (PDEs) [10].

Apart from the problem mentioned above, IDA-PBC is a constructive nonlinear feedback technique physically-inspired by energy-shaping and damping injection [11]. We have recently applied this technique to balance an unstable autonomous bicycle [12]. An advantage of this nonlinear technique is that controller parameters have a clear physical meaning thus making the implementation and tuning easier. However, the same challenge lies in solving nonlinear PDEs. The PDE problem is simplified for systems with underactuation relative degree one [13], [14]. Furthermore, the PDEs

are avoided in [15] at the cost of tuning more parameters. The IDA-PBC with integral action can deal with unknown disturbance for a robot manipulator on a flexible base [16], but there is still a gap between theory and practice.

B. Contribution

Our contributions are as follows.

Major contribution: To balance the novel-designed wheel-legged robot, the nonlinear controller IDA-PBC for the position regulation problem in the past literature is redesigned for the velocity tracking problem. The nonlinear controller is implemented in practice, and various experiments validate the stability and robustness of the controller.

Minor contribution: For the problem when the equilibrium pitch angle is unknown, linear output regulation is applied to regulate the robot stand still, and is tested in the experiment.

II. DYNAMIC MODEL

A. Mechanical Structure

The novel wheel-legged robot in Fig.1 is composed of one floating-based body, two legs ending with active wheels and one balancing tail ending with passive wheel. The coordinate of the robot system is shown in Fig.1a. A core innovation of the mechanical structure is the planar parallel mechanism at two legs. The parallel-type leg has five revolitional joints, which has two translational degrees-of-freedom along with longitudinal (x) and vertical (z) direction, respectively. Compared with serial mechanisms, this parallel mechanism presents the characteristics of compact structure, high stiffness and high load capacity. As a result, the robot may jump higher and overcome obstacles flexibly.

B. Simplification and Assumption

In this work, we focus on the balance control of the robot in the longitudinal direction. We control the motors on wheels to balance the robot. The four motors at the body frame is used to change the height of the robot (see Fig.1a and Fig.1b). The balancing tail is fixed under the floating-based body. The foot motors are capable to stabilize the robot individually, so the state-of-art whole-body control for all the motors is not considered to avoid redundant complexity.

When the robot runs along the x direction, we assume it is symmetric on y (lateral) direction. In addition, the weight of the robot is mainly concentrated in the body and wheels. Henceforth, the robot can be approximated as an inverted pendulum on a cart (IPC) of which the dynamics is

$$\begin{aligned} (M+m)\ddot{x} + ml \cos(\theta)\ddot{\theta} - ml \sin(\theta)\dot{\theta}^2 &= u, \\ ml \cos \ddot{x} + ml^2\ddot{\theta} - mgl \sin(\theta) &= 0, \end{aligned} \quad (1)$$

where M and m are the point mass concentrated at the tip of the rod and the mass of the cart, corresponding to the upper part and the wheels of the robot respectively; l is the length of the pendulum, corresponding to the height of the robot. θ is the pitch angle; x is the displacement along x direction, and u is the force on the cart. The relationship between u and the torque applied to the wheel can be established easily.

Different from the past literature on IPC, firstly, the length of the pendulum is variant, since the robot changes its height while running. Secondly, the initial state is outside the feasibility region of the linear controller, since the robot start from a large pitch angle far away from the equilibrium.

C. Linearized Model

The IPC (1) is linearized around upward equilibrium as

$$\dot{\xi} = A\xi + Bu, \quad (2)$$

where $\xi = [\theta \dot{\theta} x \dot{x}]^T$ is the state, and

$$A = \begin{bmatrix} 0 & 1 & 0 & 0 \\ \frac{M+m}{Ml}g & 0 & 0 & 0 \\ 0 & 0 & 0 & 1 \\ -\frac{m}{M}g & 0 & 0 & 0 \end{bmatrix}, \quad B = \begin{bmatrix} 0 \\ -\frac{1}{Ml} \\ 0 \\ \frac{1}{M} \end{bmatrix}.$$

D. Partial-Feedback Linearization based Model

We consider the partial feedback linearization model [17]. In (1), let

$$u = ml \left(\frac{g}{l} \cos(\theta) \sin(\theta) - \sin(\theta)\dot{\theta}^2 + \frac{\sin^2(\theta) + M/m}{l} \nu \right), \quad (3)$$

where ν is the control action from the outer loop controller, and then the partial feedback-linearized model is

$$\ddot{\theta} = \frac{g}{l} \sin(\theta) - \frac{1}{l} \cos(\theta) \nu \quad (4a)$$

$$\ddot{x} = \nu \quad (4b)$$

III. LINEAR OUTPUT REGULATION

A. Problem Formulation

In previous sections, the pitch angle θ is an ideal value that fits with the mathematical model. However, the measurement of θ by the inertial measurement unit (IMU) may deviate from the true value, and it can be expressed as

$$\tilde{\theta} = \theta + d,$$

where d is the difference. As a result, with respect to the measurement from IMU, the equilibrium of the robot is at $\tilde{\theta} = d$. In other words, (2) is equivalent to

$$\dot{\tilde{\xi}} = A\tilde{\xi} + Bu + E_d d, \quad (5)$$

where $\tilde{\xi} = [\tilde{\theta} \dot{\tilde{\theta}} x \dot{x}]^T$ (note that $\dot{\tilde{\theta}} = \dot{\theta}$), and $E_d = [0 \quad -\frac{M+m}{Ml}g \quad 0 \quad \frac{m}{M}g]^T$.

Making the robot standstill is equivalent to regulating $\dot{\theta} \rightarrow 0$ and $\dot{x} \rightarrow 0$. Alternatively, we regulate the output to zero,

$$y = \begin{bmatrix} \dot{\theta} \\ \dot{x} \end{bmatrix} = C\tilde{\xi}, \quad (6)$$

where $C = \begin{bmatrix} 0 & 1 & 0 & 0 \\ 0 & 0 & 0 & 1 \end{bmatrix}$.

B. Observer Design

We use the well-known Luenberger observer to estimate the disturbance d . It is nontrivial because d varies when the robot changes its height. Here, we choose $\tilde{\theta}$ and x as the measurement outputs

$$\mathbf{y}_m = \begin{bmatrix} \tilde{\theta} \\ x \end{bmatrix} = \mathbf{C}_m \tilde{\boldsymbol{\xi}}, \quad (7)$$

$$\text{where } \mathbf{C}_m = \begin{bmatrix} 1 & 0 & 0 & 0 \\ 0 & 0 & 1 & 0 \end{bmatrix}.$$

Then, the observer system is expressed as

$$\dot{\tilde{\boldsymbol{\xi}}} = \widehat{\mathbf{A}}\tilde{\boldsymbol{\xi}} + \widehat{\mathbf{B}}u + \mathbf{L}(\mathbf{y}_m - \widehat{\mathbf{C}}\tilde{\boldsymbol{\xi}}), \quad (8)$$

where $\tilde{\boldsymbol{\xi}} = [\tilde{\theta} \ \dot{\tilde{\theta}} \ \hat{x} \ \hat{d}]^T$ is the state of the observer, $\widehat{\mathbf{A}} = [\mathbf{A} \ \mathbf{E}_d]$, $\widehat{\mathbf{B}} = [\mathbf{B}^T \ 0]^T$ and $\widehat{\mathbf{C}} = [\mathbf{C}_m \ \mathbf{0}]$. It is clear that $(\widehat{\mathbf{A}}, \widehat{\mathbf{C}})$ is observable. The matrix \mathbf{L} is the observer gain.

C. Output Regulation

In this work, we control the robot to stand still by linear output regulation controllers. The core methodology of linear output regulation is to introduce the disturbance to the state (e.g. $\tilde{\eta}$ to $\hat{\eta}$). Using the new state, after taking the static gain controller, the state-space of the closed-loop error system is valid. Then, by making the state matrix Hurwitz, the output error is proved to decay asymptotically. In addition, the unknown disturbance can be estimated by an observer.

Following the procedure in [6], the linear controller

$$u = \mathbf{K}\widehat{\boldsymbol{\xi}}, \quad (9)$$

is considered, where $\mathbf{K} = [k_x \ k_d]$ is the tunable gain matrix. For the system in (5), (6), the output $\dot{\theta} \rightarrow 0$ and $\dot{x} \rightarrow 0$ if and only if there exists and a unique vector \mathbf{X}_c such that

$$\mathbf{0} = \begin{bmatrix} \mathbf{A} & \mathbf{BK} \\ \mathbf{LC}_m & \widehat{\mathbf{A}} + \widehat{\mathbf{B}}\mathbf{K} - \mathbf{LC} \end{bmatrix} \mathbf{X}_c + \begin{bmatrix} \mathbf{E}_d \\ \mathbf{0} \end{bmatrix}, \quad (10a)$$

$$\mathbf{0} = [\mathbf{C} \ \mathbf{0}] \mathbf{X}_c. \quad (10b)$$

These two equations imply the stability of the closed-loop error system. Refer to [6] for detailed derivations.

IV. ENERGY AND PASSIVITY BASED CONTROL

A. IDA-PBC for position regulation

The main objective of the PBC for position regulation is to shape the potential energy of the system, such that the equilibrium point of the closed-loop system corresponds to the minimum potential energy. Hence, the system can be stabilized to its equilibrium point. However, for underactuated system, its potential energy is often coupled with kinetic energy. As a result, the kinetic energy of the closed-loop system should be designed as well.

For the system (4), the total energy can be expressed in Hamiltonian form as $H(\mathbf{q}, \mathbf{p}) = \frac{1}{2}\mathbf{p}^T \mathbf{M}_I^{-1}(\mathbf{q})\mathbf{p} + V(\mathbf{q})$, where $\mathbf{q} = [\theta \ x]^T$, the inertia matrix $\mathbf{M}_I = [1 \ 0; 0 \ 1]$, thus $\mathbf{p} = [\dot{\theta} \ \dot{x}]^T$, and potential energy $V = \cos(\theta)g/l$. In order to regulate the closed-loop system to its equilibrium,

$\mathbf{p} = [0 \ 0]^T$, $\mathbf{q} = [0 \ x^*]^T$, where x^* is the target position. The target energy of the closed-loop system can be designed as $H_d(\mathbf{q}, \mathbf{p}) = \frac{1}{2}\mathbf{p}^T \mathbf{M}_d^{-1}(\mathbf{q})\mathbf{p} + V_d(\mathbf{q})$. If V_d is minimal at $\mathbf{q}^* = [0 \ x^*]^T$ with \mathbf{M}_d being positive-definite in a neighborhood of \mathbf{q}^* , then by considering H_d as the Lyapunov function, it can be proved that the equilibrium \mathbf{q}^* is stable with the neighborhood being the domain of attraction.

Among different approaches of PBC, IDA-PBC in [11] with solution [13] realize the stabilization of the nonlinear system (4). In this approach, $V_d(\mathbf{q}) = \frac{3gl}{k \cos^2(\theta)} + \frac{P}{2} \left[x - x^* + 3l \ln(\sec(\theta) + \tan(\theta)) + \frac{6lm_{22}^0}{k} \tan(\theta) \right]^2$, which has minimum at $\mathbf{q}^* = [0 \ x^*]^T$. $\mathbf{M}_d = \begin{bmatrix} m_{11} & m_{12} \\ m_{12} & m_{22} \end{bmatrix} = \begin{bmatrix} \frac{k}{3l^2} \cos^3(\theta) & -\frac{k}{2l} \cos^2(\theta) \\ -\frac{k}{2l} \cos^2(\theta) & k \cos(\theta) + m_{22}^0 \end{bmatrix}$ with free parameters $k > 0$ and $m_{22}^0 \geq 0$. It is positive-definite in the range $\theta \in (-\frac{\pi}{2}, \frac{\pi}{2})$, which is the domain of attraction. The corresponding controller, IDA-PBC, is

$$\nu = A_1(\theta)P(x - x^*) + \mathbf{p}^T A_2(\theta)\mathbf{p} + A_3(\theta) - k_v A_4(\theta)\mathbf{p}, \quad (11)$$

where $\mathbf{G} = [-\cos(\theta)/l \ 1]^T$, $k_v > 0$, $P > 0$ are free parameter. In addition,

$$A_1 = - \left(m_{12} \frac{dF}{d\theta} + m_{22} \right), \quad (12a)$$

$$A_2 = -\frac{1}{2} m_{12} \mathbf{M}_d^{-1} \begin{bmatrix} \frac{dm_{11}}{d\theta} - \alpha_{11} & \frac{dm_{12}}{d\theta} \\ \frac{dm_{12}}{d\theta} - \alpha_{12} & \frac{dm_{22}}{d\theta} \end{bmatrix} \mathbf{M}_d^{-1}, \quad (12b)$$

$$A_3 = m_{12} \frac{6gl \sin(\theta)}{k \cos^3(\theta)} + PF(\theta)A_1, \quad (12c)$$

$$A_4 = \begin{bmatrix} -\frac{\cos(\theta)}{l} & 1 \end{bmatrix} \mathbf{M}_d^{-1}, \quad (12d)$$

where

$$F(\theta) = 3l \ln(\sec(\theta) + \tan(\theta)) + \frac{6lm_{22}^0}{k} \tan(\theta),$$

$$\boldsymbol{\alpha} = \begin{bmatrix} \alpha_{11} \\ \alpha_{12} \end{bmatrix} = \frac{-k^2 \cos^3(\theta) \sin(\theta)}{12l^2} \begin{bmatrix} \frac{\cos(\theta)}{l} \\ -1 \end{bmatrix}.$$

B. IDA-PBC for velocity track

Instead of regulating the robot to a specific position, we expect the wheel-legged robot to move at a constant velocity given by the remote controller. Therefore, we convert the IDA-PBC for velocity track.

First of all, the steady state at $[\theta \ \dot{\theta} \ \dot{x}]^T = [0 \ 0 \ \dot{x}^*]^T$ is valid when $\nu = 0$, because an unforced system with a constant velocity can be stable.

As shown in the position regulation, $x - x^*$ only occurs in V_d , which has the minimum at x^* . Equivalently, we can redesign V_d by removing $x - x^*$ directly. Then, the minimum of V_d is still $\theta = 0$, and the total energy is not related with x . As a result, the first term in (11) would disappear. Meanwhile, it is valid to define \bar{p} as $[\theta \ \dot{x}_{err}]$, where $\dot{x}_{err} = \dot{x} - x^*$, to convert the previous position regulation problem to velocity regulation problem. Then, the energy function of the robot is $H(\mathbf{q}, \mathbf{p}) = \frac{1}{2}\bar{\mathbf{p}}^T \mathbf{M}_I^{-1}(\mathbf{q})\bar{\mathbf{p}} + V(\mathbf{p})$, which means that the corresponding Lyapunov function H_d is shifted horizontally

by \dot{x}^* in \dot{x} direction, i.e. $H_d(\mathbf{q}, \bar{\mathbf{p}}) = \frac{1}{2}\bar{\mathbf{p}}^T \mathbf{M}_d^{-1}(\mathbf{q})\bar{\mathbf{p}} + V_d(\mathbf{q})$. Moreover, as \mathbf{M}_d is independent with \dot{x} , dH_d/dt is still negative in the same sense but with \dot{x} being \dot{x}_{err} . Finally, the equilibrium moves to $[\theta \ \dot{\theta} \ \dot{x}]^T = [0 \ 0 \ \dot{x}^*]^T$.

As discussed above, the IDA-PBC for velocity track is

$$\nu = \bar{\mathbf{p}}^T A_2(\theta)\bar{\mathbf{p}} + A_3(\theta) - k_v A_4(\theta)\bar{\mathbf{p}}. \quad (13)$$

V. EXPERIMENTS

A. Experimental Setup

Several experiments are conducted to test the stability and performance of our linear output regulation and nonlinear IDA-PBC. All parameters are listed in Table.I.

Parameters	
Robot/IPC	$m = 11kg; M = 3kg; g = 9.81m/s^2$ $0.37m \leq l \leq 0.7m; r_w = 0.1m; d_w = 0.47m$
IDA-PBC	$k = 0.015; m_{22}^0 = 0.04; k_v = 0.05; P = 0.2$
Output regulation	$\mathbf{k}_x = [150 \ 12 \ 0.001 \ 10]; k_d = -167;$ $\mathbf{L} = [27.63 \ 397.75 \ -6.48 \ -111.4 \ -0.45]^\top$

TABLE I: Parameters

In the table, r_w and d_w denote the radius of the wheel and the distance between the two wheels respectively. The height l is calculated in real-time using the angles of body motors and the lengths of leg links. The gain matrix \mathbf{k}_x in output regulation is calculated by LQR. It is easy to prove that (10) is solvable with the parameters above. Particularly, we set the third element of \mathbf{k}_x as a small value because it is more practical in experiment to track a velocity reference instead of staying at a specific position.

We measure the pitch angle θ and the roll angle ϕ with their velocities by the IMU. Meanwhile, the angular velocities of the motor at the right wheel ω_r (rad/s) and left wheel ω_l (rad/s) are measured by the motor encoder. Then, the linear velocity \dot{x} and the yaw velocity $\dot{\gamma}$ of the robot are calculated by $\dot{x} = \frac{\omega_r + \omega_l}{2}r_w, \dot{\gamma} = \frac{\omega_r - \omega_l}{d_w}r_w$. The propulsive force u in the model of IPC (1) and (2) is converted to the torque applied to each foot motor by $\tau = \frac{1}{2}r_wu$. Moreover, the yaw torque $\tau_\gamma = 0.3(\dot{\gamma} - \dot{\gamma}^*)$ is added to and subtracted from τ of the left and right motors respectively to make the robot rotate, where $\dot{\gamma}^*$ is the reference yaw velocity given by the remote controller. As the yaw torque does not change the total torque in x direction, it will not break the balance.

In the experiment, CPU PICO-WHU4 is used. The control period is set as $T_s = 2$ ms. Hence, we calculate x as $x_k = x_{k-1} + T_s \dot{x}_{k-1}$, and discretize the observer as

$$\hat{\zeta}_k = (I + T_s \hat{\mathbf{A}}) \hat{\zeta}_{k-1} + T_s \hat{\mathbf{B}} u_{k-1} + T_s \mathbf{L} (\mathbf{y}_{m,k-1} - \hat{\mathbf{C}} \hat{\zeta}_{k-1}).$$

B. Experiments

Eight experiments are conducted to test the stability performance of the controllers. Photos are attached in Fig.2.

1) Starting up: The robot starts from its initial posture (Fig. 2a) to its balance posture (Fig. 2b) under the minimum height. Both nonlinear controller IDA-PBC in (13) and linear controller $u = \mathbf{k}_x \tilde{\xi}$ (\mathbf{k}_x in Table.I, $\tilde{\xi}$ in (5)) are applied, and the performance are compared.

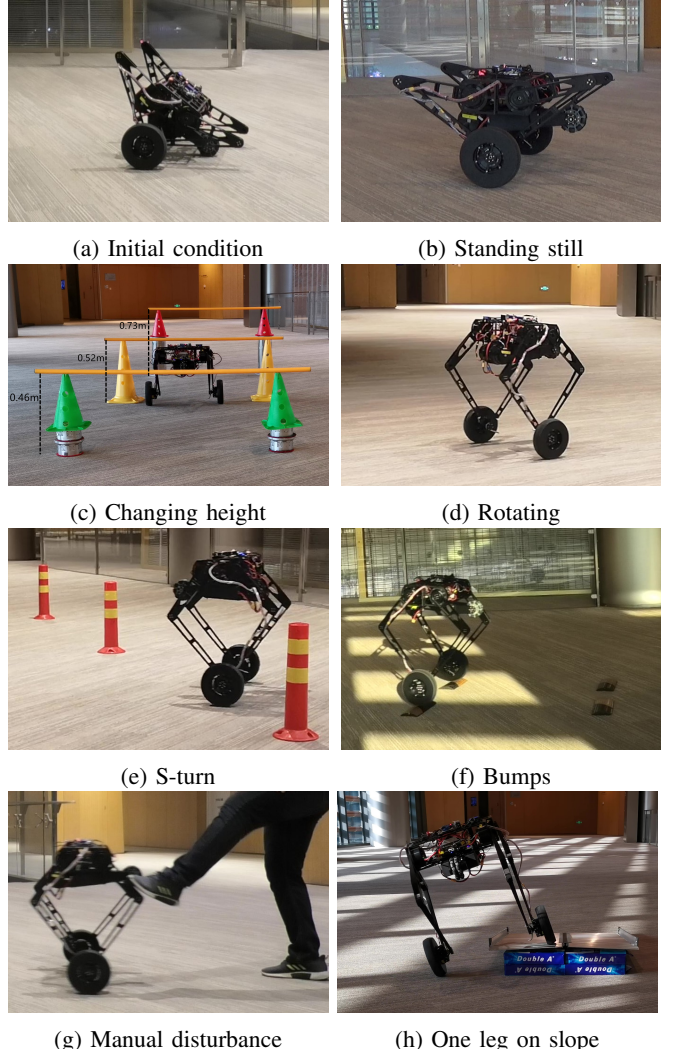


Fig. 2: Photos of the experiments. These and many more maneuvers in action are shown in the accompanying video.

2) Standing still: Linear output regulation with observer is used to make the robot stand still (Fig. 2b) without moving forward and backward.

3) Changing height: The robot changes its height when moving in straight lines to avoid the beams at different heights (Fig. 2c). IDA-PBC (13) is used to achieve angle regulation ($\theta, \dot{\theta}$) and velocity track (\dot{x}).

4) Rotating: The robot rotates in a circle at the maximum height (Fig.1) with IDA-PBC (13). The result proves that the rotation in the yaw direction does not influence the balance control in the longitudinal direction.

5) S-turn: The robot takes S-turns around piles at the maximum height (Fig.2e) with IDA-PBC (13). It can be considered as a combination of straight-line moving and circular rotating, so the control performance of IDA-PBC is tested with movement in both directions.

6) Bump: The robot runs over speed bumps by IDA-PBC (13). It tests the robustness of IDA-PBC when external disturbances are added to the wheels (bottom) of the robot.

7) Manual disturbance: The robot keeps balance by IDA-PBC (13) when two experimenters kick its body on both

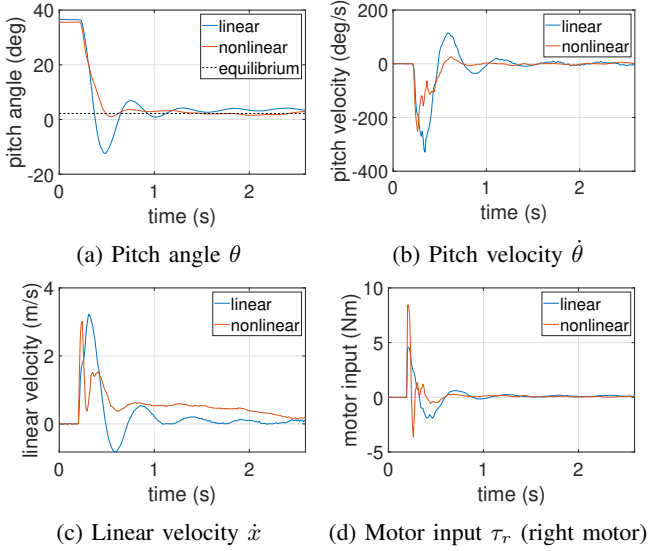


Fig. 3: Starting up

sides. It tests the robustness of IDA-PBC when external disturbances are added to the body (top) of the robot.

8) One leg on slope: The robot rushes on a small slope ($1.2m$ with 7°) with one leg on the slope and falls to the ground. It tests the robustness of IDA-PBC when one wheel is off ground slightly.

C. Results

The experimental results are discussed individually, where the unit of angles is converted to degree for simple reading.

1) *Starting up*: As shown in Fig.3a, the initial angle is around 36° , which is outside the linear region. In consequence, the pitch angle is less oscillating and reaches the equilibrium faster in the case of using the nonlinear controller. The overshoot is 1° by IDA-PBC, while it is 12° by linear control. Similar phenomena happen to $\dot{\theta}$ (Fig.3b). In Fig.3c, the robot stops slower with nonlinear controller, but the response of the pitch angle is more addressed here.

Particularly, the control action by the nonlinear controller changes more aggressively than that by linear controller (Fig.3d). This realizes the little overshoot by the nonlinear controller. It would be possible to achieve similar results by the linear controller if it is tuned as a fuzzy controller [18], [19]. Nevertheless, a major limitation of the linear controller is that its parameters (fuzzy membership function) should be re-tuned when the height of the robot changes.

2) *Standing still*: In the result, the measured states are compared with its observed value in Fig.4. Here, we assume that the initial values of \hat{x} , $\hat{\dot{x}}$, $\hat{\theta}$ and $\hat{\dot{\theta}}$ are known exactly, but approximately estimate the initial value of \hat{d} as 2.7° .

First of all, it must be pointed out that an IPC can hardly stand still on the smooth ground in practice. However, due to the friction between the wheels and the carpet, the robot is possible to stand still (see the zero linear velocity in Fig.4d).

Due to the same reason, the estimated states will differ from the real values. In detail, the motor input (Fig.4f) is nonzero, so the estimated acceleration should be nonzero by

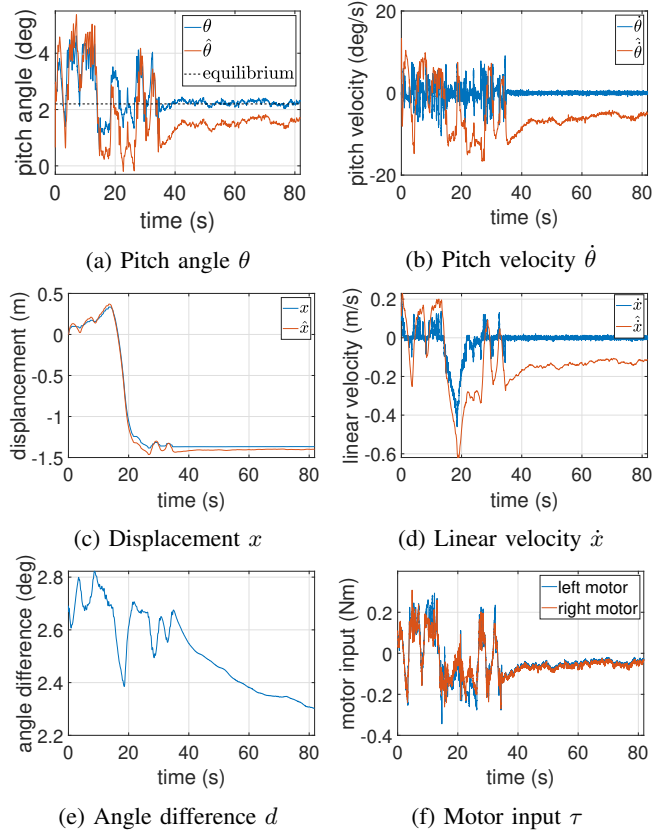


Fig. 4: Standing still

mathematical model. However, the robot does not move in reality due to the friction. This mismatch brings the error in the acceleration, which in turn is integrated to the velocity ($\hat{\dot{\theta}}$ and $\hat{\dot{x}}$ in Fig.4b and Fig.4d respectively) and the position ($\hat{\theta}$ and \hat{x} in Fig.4a and Fig.4c respectively). However, the last term in ξ_k would regulate the estimated value to its real value. As shown in Fig.4b, 4d, 4e, the estimated values are approaching to the real values (d is about 2.2°). Similarly, the motor deadzone also leads to the errors in state observer.

3) *Changing height*: As indicated in Fig.5a, the robot passes three beams with the height $0.7m$, $0.52m$ and $0.37m$, and runs backward with the height $0.37m$, $0.52m$ and $0.7m$. The moving direction is indicated by the linear velocity in Fig.5b. In this experiment, as the robot moves slowly, the influence on the velocity track performance caused by the sudden variation of the height is not deliberated. In this experiment, the robot is stable when it is running in the straight line. Moreover, the parameter l in the controller (13) is changed according to the actual height of the robot.

4) *Rotating*: As discussed in Sec.V-A, the yaw torque does not influence the balance control, so the robot rotates clockwise at the velocity of $165^\circ/s$ smoothly. The torques applied to wheel motors are also smooth (Fig.6b).

5) *S-turn*: As shown in Fig.7b, the robot turns anticlockwise at the first and third piles and turns clockwise at the second pile. Nevertheless, to keep the robot on the desired path, the experimenter tunes the remote controller frequently. The poor smoothness of the reference signal results in the

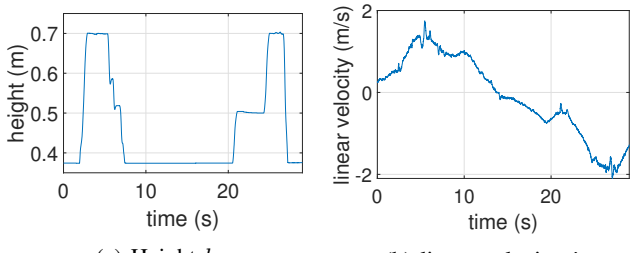


Fig. 5: Changing height

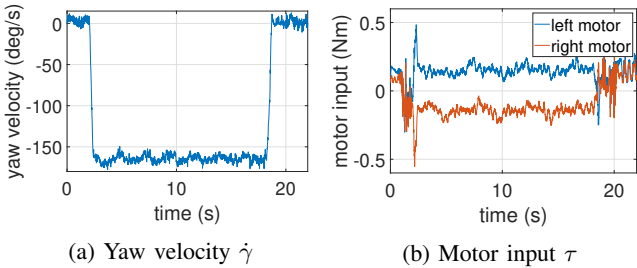


Fig. 6: Rotating

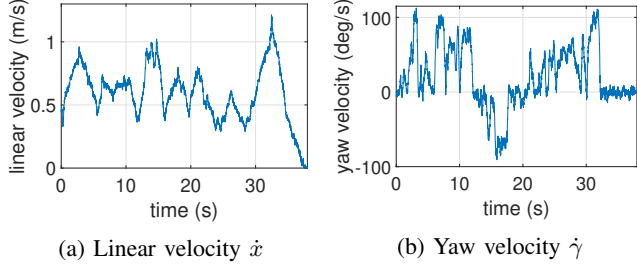


Fig. 7: S-turn

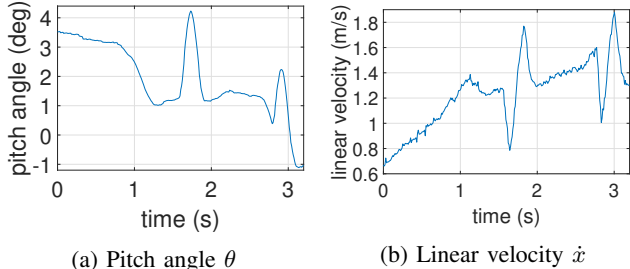


Fig. 8: Bumps

oscillation in \dot{x} (Fig.7a) and $\dot{\gamma}$ (Fig.7b) as well. Despite the imperfect smoothness, the robot keeps stable when following a desired path at its maximum height.

6) Bumps: In Fig.8, the robot reaches the first bump at 1.5s and the second bump at 2.8s. It is clear from Fig.8a, 8b, although both the pitch angle and the linear velocity change sharply at the bumps, the robot keeps stable after leaving the bumps. The result implies that the IDA-PBC is robust to such exogenous disturbance on the wheels.

7) Manual disturbance: In Fig.9b, each 0 crossing indicates a kick on the robot, where the robot is stopped and changes its direction. After each kick, the robot accelerates suddenly due to the kick, and then decelerates quickly because IDA-PBC regulates the speed to zero. Before the

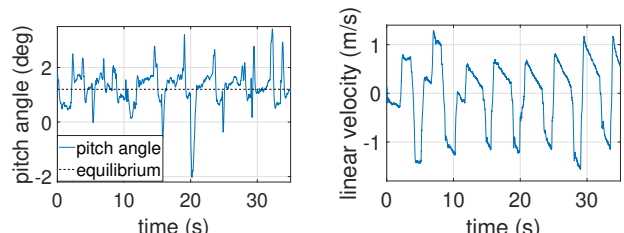


Fig. 9: Manual disturbance

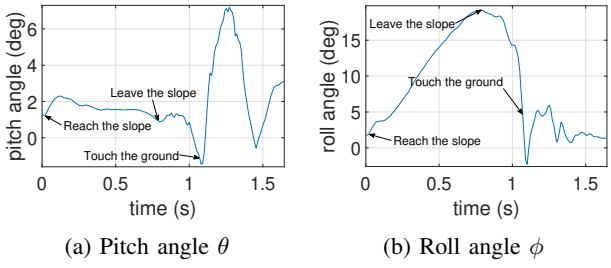


Fig. 10: One leg on slope

speed reduces to zero, the robot is kicked on the other side. Similar phenomenon happens to the pitch angle (Fig.9a), which changes suddenly due to the kick, and then returns to its equilibrium (about 1.2°) quickly. The results indicate the good robustness of IDA-PBC to manual disturbances on robot body and thighs.

8) One leg on slope: Although the control algorithm is not designed for slope, the robot can rush on a small slope. As shown in Fig.10b, the roll angle increases to 19° when the robot moves on the slope, the projection of the center of mass may keep between the two wheels, and the robot keeps stable and moves in a straight line. After the wheel leaves the top of the slope and falls on the ground, the robot is still stable especially if its height decreases. As shown in Fig.10a, the pitch angle converges to its equilibrium (2.2°). The result verifies the robustness of IDA-PBC when the robot is running fast and one wheel is off the ground slightly.

VI. CONCLUDING REMARKS

In this paper, in order to balance the novel wheel-legged robot, there are two challenges: 1) how to maintain the standing of robots without moving forward or backward mightily when the equilibrium of the pitch angle is unknown; 2) how to balance the robot when the initial state of the robot is far away from the equilibrium or the height is changing. For the first challenge, the linear output regulation technique along with LQR is adopted to balance the robot. For the second challenge, based on the nonlinear dynamic model of the robot, IDA-PBC is applied to balance the robot and track a constant velocity given by a remote controller. The efficacy and robustness of the proposed control methodologies have been validated by experimental results in various tasks.

We are mounting a manipulator to this wheel-legged robot to accomplish more complex tasks. More details will be presented in a future paper.

REFERENCES

- [1] HandleTM. [Online]. Available: www.bostondynamics.com/handle
- [2] V. Klemm, A. Morra, C. Salzmann, F. Tschopp, K. Bodie, L. Gulich, N. Küng, D. Mannhart, C. Pfister, M. Vierneisel, F. Weber, R. Deuber, and R. Siegwart, "Ascento: A two-wheeled jumping robot," in *2019 International Conference on Robotics and Automation (ICRA)*, 2019, pp. 7515–7521.
- [3] S. Wang, L. Cui, J. Lai, S. Yang, X. Chen, Y. Zheng, Z. Zhang, and Z.-P. Jiang, "Gain scheduled controller design for balancing an autonomous bicycle," in *2020 IEEE/RSJ International Conference on Intelligent Robots and Systems (IROS)*. IEEE, 2020, pp. 7595–7600.
- [4] G. Zambella, G. Lentini, M. Garabini, G. Grioli, M. G. Catalano, A. Palleschi, L. Pallottino, A. Bicchi, A. Settimi, and D. Caporale, "Dynamic whole-body control of unstable wheeled humanoid robots," *IEEE Robotics and Automation Letters*, vol. 4, no. 4, pp. 3489–3496, 2019.
- [5] V. Klemm, A. Morra, L. Gulich, D. Mannhart, D. Rohr, M. Kamel, Y. d. Viragh, and R. Siegwart, "LQR-assisted whole-body control of a wheeled bipedal robot with kinematic loops," *IEEE Robotics and Automation Letters*, vol. 5, no. 2, pp. 3745–3752, 2020.
- [6] J. Huang, *Nonlinear Output Regulation*. Society for Industrial and Applied Mathematics, 2004.
- [7] A. Isidori and C. I. Byrnes, "Output regulation of nonlinear systems," *IEEE transactions on Automatic Control*, vol. 35, no. 2, pp. 131–140, 1990.
- [8] A. Laib, "Adaptive output regulation of robot manipulators under actuator constraints," *IEEE Transactions on Robotics and Automation*, vol. 16, no. 1, pp. 29–35, 2000.
- [9] S. T. Wu and Y. C. Chuang, "Output regulation of robot manipulators with a constantly revolving arm," *IEEE Transactions on Robotics and Automation*, vol. 19, no. 6, pp. 1002–1006, 2003.
- [10] T. J. Tarn, P. Sanposh, D. Cheng, and M. Zhang, "Output regulation for nonlinear systems: some recent theoretical and experimental results," *IEEE Transactions on Control Systems Technology*, vol. 13, no. 4, pp. 605–610, 2005.
- [11] R. Ortega, M. W. Spong, F. Gomez-Estern, and G. Blankenstein, "Stabilization of a class of underactuated mechanical systems via interconnection and damping assignment," *IEEE Transactions on Automatic Control*, vol. 47, no. 8, pp. 1218–1233, 2002.
- [12] L. Cui, S. Wang, J. Lai, X. Chen, S. Yang, Z. Zhang, and Z.-P. Jiang, "Nonlinear balance control of an unmanned bicycle: Design and experiments," in *2020 IEEE/RSJ International Conference on Intelligent Robots and Systems (IROS)*. IEEE, 2020, pp. 7279–7284.
- [13] J. A. Acosta, R. Ortega, A. Astolfi, and A. D. Mahindrakar, "Interconnection and damping assignment passivity-based control of mechanical systems with underactuation degree one," *IEEE Transactions on Automatic Control*, vol. 50, no. 12, pp. 1936–1955, 2005.
- [14] Z.-P. Jiang and I. Kanellakopoulos, "Global output-feedback tracking for a benchmark nonlinear system," *IEEE Transactions on Automatic Control*, vol. 45, no. 5, pp. 1023–1027, 2000.
- [15] A. Donaire, R. Mehra, R. Ortega, S. Satpute, J. G. Romero, F. Kazi, and N. M. Singh, "Shaping the energy of mechanical systems without solving partial differential equations," *IEEE Transactions on Automatic Control*, vol. 61, no. 4, pp. 1051–1056, 2016.
- [16] Y. R. Teo, A. Donaire, and T. Perez, "Regulation and integral control of an underactuated robotic system using IDA-PBC with dynamic extension," in *2013 IEEE/ASME International Conference on Advanced Intelligent Mechatronics*, 2013, pp. 920–925.
- [17] M. W. Spong, *Robot Dynamics and Control*, 1st ed. John Wiley & Sons, Inc., 1989.
- [18] D. Sáez and A. Cipriano, "Fuzzy linear quadratic regulator applied to the real time control of an inverted pendulum," *IFAC Proceedings Volumes*, vol. 31, no. 4, pp. 155 – 160, 1998, 5th IFAC Workshop on Algorithms & Architecture for Real Time Control (AARTC'98), Cancun, Mexico, 15-17 April 1998. [Online]. Available: <http://www.sciencedirect.com/science/article/pii/S1474667017421501>
- [19] A. I. Roose, S. Yahya, and H. Al-Rizzo, "Fuzzy-logic control of an inverted pendulum on a cart," *Computers & Electrical Engineering*, vol. 61, pp. 31 – 47, 2017. [Online]. Available: <http://www.sciencedirect.com/science/article/pii/S0045790617313654>